Available online at www.sciencedirect.com

SCIENCE DIRECT®

Polymer 46 (2005) 10226–10236

polymer

www.elsevier.com/locate/polymer

Real time observation of crystallization in polyethylene oxide with video rate atomic force microscopy

Jamie K. Hobbs[a,*], Cvetelin Vasilev[a], Andrew D.L. Humphris[b]

[a]Department of Chemistry, University of Sheffield, Brook Hill, Sheffield S3 7HF, UK
[b]Infinitesima Ltd, Oxford Centre for Innovation, Mill Street, Oxford OX2 0JX, UK

Received 7 June 2005; received in revised form 10 August 2005; accepted 13 August 2005
Available online 6 September 2005

Abstract

Video rate atomic force microscopy (VideoAFM), with a frame rate of 14 frames/s and a tip velocity of up to 15 cms^{-1}, is used to image polyethylene oxide films during crystal growth. The capabilities of VideoAFM when applied to semicrystalline polymer surfaces are explored. Image quality comparable to that found with conventional contact AFM is achieved but with a nearly 1000 times improvement in time resolution. By applying the technique to the real-time observation of crystal growth, different modes of rapid crystallization are followed in real time. Observation of the spherulite growth front allows measurement of growth rates at the lamellar scale, from which a factor of two difference in the rate of radial growth to the rate of tangential growth is observed, confirming that the elongated nature of spherulite lamellae is due to geometric constraints rather than an inherent fibrillar character. Measurements on screw dislocation growth, when large amounts of crystallizable material is trapped at the surface show that the terrace height does not influence the rate of crystal growth, confirming that under these conditions processes at the lamellar growth front control the rate of growth. When only a thin film of molten material is left on the surface of the already crystallized film dendritic growth is observed, implying a diffusion controlled process under these far from equilibrium conditions.

Keywords: Polyethylene oxide; Crystallization; AFM

1. Introduction

Polymer crystallization is a process that occurs far from equilibrium, with kinetics controlling both the final structure and the route that is taken to that structure. Recent simulations and models (e.g. Refs. [1–3]) have aimed to capture the crystallization kinetics at the molecular scale, and provided new insights into old questions, such as what factors control the crystal thickness [4]? At the same time, modern synchrotron and lab-based X-ray scattering instrumentation has allowed crystallization to be followed at the unit-cell to lamellar scale with second time resolution (e.g. Refs. [5–7]). However, by the very nature of kinetically controlled processes, it is the specifics, and in particular rare events (such as nucleation), which play a disproportionate role in the final structure, and to access these events unambiguously requires a real-space technique. Polymer crystallization at surfaces has been extensively studied (e.g. Refs. [8–10]), with particular focus on the possible orienting effect of free surfaces on polymer chains, leading to a change in the crystallization behaviour compared to that in the bulk. As polymers are frequently used in thin-film coatings and similar applications, the way in which the surface impacts on crystallization is of interest both fundamentally, and for commercial reasons.

Atomic force microscopy (AFM) has been increasingly used in recent years both for observation of crystallization in real-time, and for ex situ study [11–16]. Although limited to imaging the surface or near surface region, the strength of the method is that, as a non-destructive technique, real-time data can be obtained. The use of high temperature stages has allowed many polymers to be imaged during both crystallization and melting [12,15,17]. Polyethylene oxide has received particular attention, with crystallization in relatively thick films (where the relationship to bulk crystallization has been stressed) [12,18,19], as well as in

---

* Corresponding author. Tel.: +44 114 2229316.
E-mail address: jamie.hobbs@sheffield.ac.uk (J.K. Hobbs).

0032-3861/$ - see front matter © 2005 Elsevier Ltd. All rights reserved.
doi:10.1016/j.polymer.2005.08.042

thin films [20] and adsorbed monolayers [16,21], forming subjects for study. One of the main drawbacks of AFM when used for such studies is the relatively slow rate of data acquisition. Although, for ex situ use it has proved a powerful tool, in situ observations have largely been limited to very small supercoolings, where crystallization typically forms very large and infrequently branching crystals, or very large supercoolings where crystallization close to the glass transition temperature occurs in a regime dominated by material transport. Considering the exponential supercooling dependence of growth rate, and the minute timescale of AFM imaging, this is understandable.

Since the early 1990s, there has been a concerted effort to improve the imaging rate of AFMs, with some success [22–25]. These attempts have tackled the two main hindrances of faster scanning—the mechanics of the scan-stage, and the bandwidth of the cantilever-feedback loop system. For imaging processes in soft, biological samples, there have been some outstanding improvements in image rate, with sub-100 ms timescales becoming accessible [25]. This instrument, which includes a complete re-design of the microscope mechanics so as to optimise every component for faster scanning, is limited in the maximum scan area obtainable, making its application to processes at length scales above the molecular difficult. A second approach has been to incorporate actively controlled cantilevers [22,26] into conventional microscopes, giving maximum tip-velocities similar or greater than those in [25], but with the limitation that the actual frame-rate is still 10 s of seconds.

We have adopted a different approach, in which a microresonator is used as a scan-stage [27], and incorporating a ‘passive mechanical feedback loop’ with a bandwidth of ∼2 MHz [28]. This has achieved the fastest AFM scan-rates to-date, 35 images/s. The cantilever tracks the surface using an adaptation to conventional, constant height (feedback free) contact mode. As detailed in [28], there is no electronic feedback loop, but rather by controlling the mechanics of the cantilever, combined with an additional (constant) force applied directly to the tip end of the cantilever, the tip is made to track the sample surface. The image itself consists of the high frequency optical deflection of the AFM cantilever, which is collected and displayed in real-time.

In this paper, we use the VideoAFM to bridge the gap in information on crystal growth kinetics between the data supplied by optical microscopy at high growth rates but with low (∼1 μm) lateral spatial resolution, and that supplied by conventional AFM with high spatial resolution (∼10 nm) but poor temporal resolution and hence slow (less than 50 nm s^{-1}) growth rates. As polymer crystal growth is a kinetically controlled process, it is, a priori, unclear whether observations at the nanometre scale made when the growth rate is slow can be assumed to hold true under other crystallization conditions when growth is fast.

2. Experimental details

The polyethylene oxide (PEO) polymer samples used in this studies were standards obtained from Polymer Laboratories Ltd, M_w 220,000 g/mol, $M_w/M_n \sim 1.1$, denoted PEO220 in the following, and M_w 50,000 g/mol, $M_w/M_n \sim 1.1$, denoted PEO50 in the following. The polymer samples and toluene (Fisher Scientific) were used without further purification. All samples were drop-cast from a dilute toluene solution (concentration of about 2 mg/ml) onto glass cubes ($1\times1\times1$ mm^3), cleaned in an ultrasonic bath in chloroform prior to the PEO film casting. The resulting thickness of the polymer films was of the order of several hundred nanometres to 1 μm.

A VideoAFM™ (Infinitesima Ltd, Oxford, UK) was used for this study. This instrument is based on the techniques outlined in [28]. The VideoAFM scan head and controller were connected to a Dimension 3100 (D3100) AFM with Nanoscope IV controller (Veeco, Santa Barbara, CA) operated in ‘contact mode’ for conventional imaging, using coated micro fabricated silicon nitride cantilevers (Infinitesima Ltd part no. VC100.130). These cantilevers allow switching between conventional contact mode imaging, and, when used in conjunction with a resonant scan-stage (see below), high speed scanning mode.

The samples (glass blocks covered by PEO film) were mounted at the ends of the legs of a microresonator giving a resonant frequency of approximately 15 kHz. All the data shown was obtained using an amplitude of oscillation of 1.5 μm, which provided the fast-scan axis for the VideoAFM with an image size of 3 μm. The data was corrected in real-time for the sinusoidal velocity, giving an undistorted image. The microresonator, in turn, was mounted on the VideoAFM scan head, which provided the slow-scan axis (14 frames/s). This sample scanning set-up was placed directly below the scan head of the D3100 AFM and provided a possibility for either conventional AFM (slow), or VideoAFM (high-speed) imaging of the sample surface. The high-speed data were acquired by the VideoAFM Workstation, the raw optical signal from the photodiode detection system of the D3100 microscope providing the image.

The high-speed sample scanning set-up together with the VideoAFM software allowed an imaging rate of 14 frames/s, giving a time resolution of approximately 70 ms between the separate frames. The lateral spatial resolution of the VideoAFM images is comparable to the lateral resolution of a conventional AFM operated in contact mode and is in the range 6–10 nm (i.e. tip limited). As the images are collected at 256×256 pixel the actual resolution obtained was 12 nm—single pixel width features are observed.

The PEO samples were imaged at elevated temperatures using a Linkam THMS 600 hot-stage with Linkam TP 93 controller in ambient atmosphere. The hot-stage heater was placed directly below the leg of the microresonator on which the sample was mounted. The samples were cooled

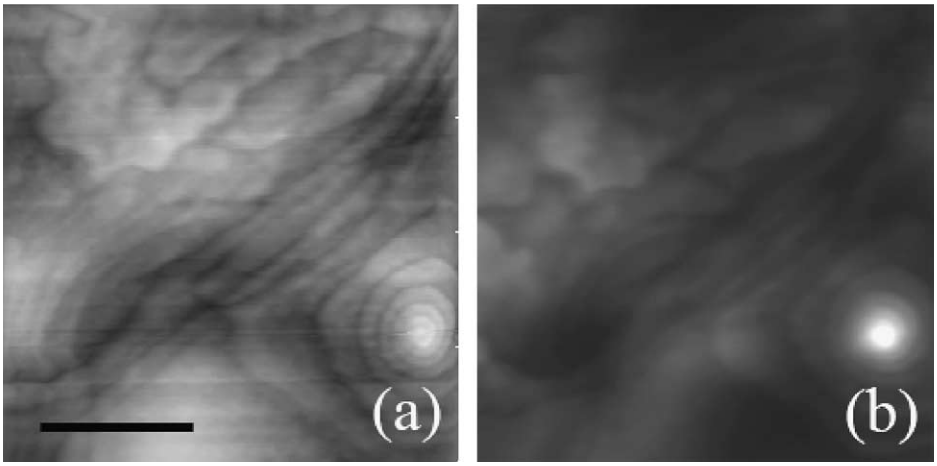

Fig. 1. (a) A VideoAFM image showing part of a polyethylene oxide (PEO220) spherulite, taken at room temperature. (b) The corresponding conventional AFM image in which black to white represents a change in height of 200 nm. (b) is a software zoom from a 15 μm image, so the pixel resolution is, a priori, not as good as that in the VideoAFM image. The scale bar represents 1 μm.

down from the molten state until the crystallization process started and then imaged under isothermal conditions. The disadvantage of this arrangement was that the temperature measured by the hot-stage controller does not represent the real sample temperature, as the heater is not in direct contact with the sample. The actual temperature of the sample stage was calibrated both by comparison between the known melting point of the polymer and that observed while imaging, as well as the optically measured spherulite growth rate, and the spherulite growth rate measured using the VideoAFM (data not shown).

The image data is collected in the form of a video (.avi) file, from which the individual bitmap images can be extracted. Here we are primarily interested in changes that occur during rapid crystallization processes. The contrast variations seen when observing the original movie file are clear because of the brain's ability to rapidly follow changes and motion—the eye naturally focuses on the moving object and sees its trajectory. When looking at extracted still images the features of interest are not always clear, so we have processed some of the images (as indicated below) to include contrast that depends on the difference between consecutive images. The method and original data are included in Appendix A.

3. Results and discussion

As the contrast mechanism in VideoAFM is somewhat different from conventional AFM, we will first consider VideoAFM imaging at room temperature where the imaging parameters are optimised, and discuss the tip-sample interaction. We will then look at data collected during crystal growth and discuss how this data contributes to our understanding of rapid crystal growth processes.

Fig. 1 shows a VideoAFM image of the surface of a polyethylene oxide sample taken after crystallization on cooling to room temperature, and a conventional AFM topographic image of the same area (note the conventional AFM is a software zoom from an image of a larger area). On static samples such as this, where the material has completed crystallization, a high level of contrast is present at steps and edges in the sample in the VideoAFM image. The image can be considered as a combination of the slope (differential, dz/dx) of the sample surface and the relative height (z) of the surface. This combination of different contrast information occurs because the AFM cantilever is responding at a frequency considerably higher than its first bending mode. Rapid changes in topography will lead to greater changes in cantilever deflection (and therefore, pixel intensity) than the same change in height but with a gentler slope, as in this latter case the length of the cantilever over which the bending is distributed is greater. The image shows the surface of a spherulite (radius top right to bottom left) with a screw dislocation overgrowth, a growth structure that is commonly observed in PEO films.

When imaging soft materials, the force applied to the surface, and the potential for damage to the sample, is of central importance. The VideoAFM uses an imaging technique similar to conventional contact mode, but with an additional direct force acting on the tip end of the cantilever to help maintain tip-sample contact. In the images obtained here, the direct force has two origins. Firstly, there is an electrostatic force that is controlled by the operator, introduced by maintaining a voltage between the gold film on the back of the cantilever and a ground plate beneath the sample. Secondly, advantage is taken of the capillary neck that naturally occurs between the tip and the surface, and provides an essentially constant attractive force between the two. These forces combine to give a total down force on the tip of 1–100 nN (depending on environmental conditions, the applied electrostatic force, the nature of the sample surface, and the radius of curvature of the probe). In the images collected here this force was estimated at 30 nN,

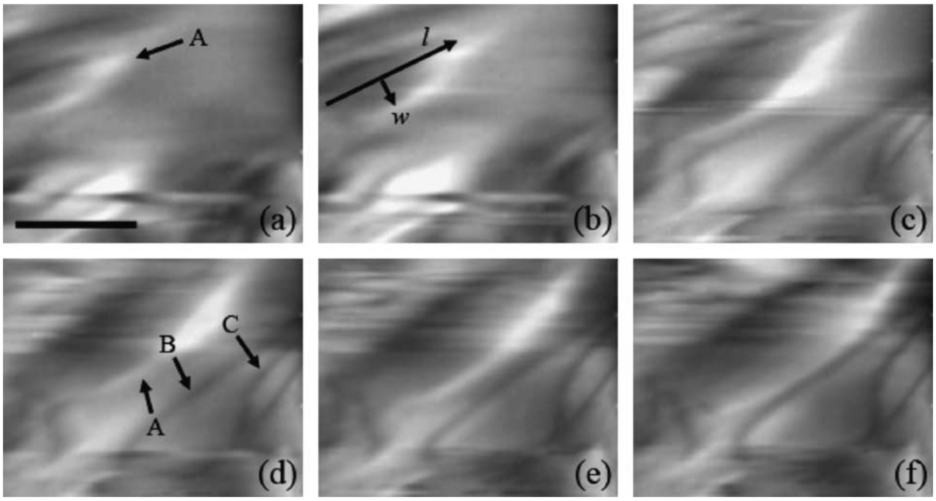

Fig. 2. A sequence of VideoAFM images showing the growth front of a PEO50 spherulite, taken at 56 °C. (a) Taken at 0 s, (b) taken at 0.49 s, (c) taken at 1.61 s, (d) taken at 2.1 s, (e) taken at 2.59 s, (f) taken at 3.08 s. 'A', 'B' and 'C' indicate lamellae referred to in the text. The arrows in (b) indicate the length (*l*) and width (*w*) of the lamella A, as referred to in the text. The scale bar represents 1 μm.

although pull-off experiments were not performed at elevated temperatures to directly measure the tip-surface force. If the sample surface is tracked by the tip in both trace and retrace (i.e. it does not lose contact with the surface), then this tip-sample interaction gives a reasonable estimate of the maximum force on the sample surface—i.e. the same as would be experienced in conventional contact mode used in standard conditions. When the probe leaves the surface, the transient force is probably higher than this. As the cantilever itself cannot be used to measure the force at these frequencies (its 'stiffness' is not a relevant parameter above its resonant frequency), we do not have a measure of the transient force—this is a subject of our current research.

All of the data shown here were obtained under conditions where the sample was not being damaged, and where no measurable influence of the imaging over the process being imaged was observed. Care was taken to scan around the area imaged to ensure that any features were representative, and not the result of the imaging process itself. As conventional contact mode imaging of PEO is possible [19,29], in contrast to many molten polymers that cannot be imaged in contact mode [30], this is an ideal polymer for such a study.

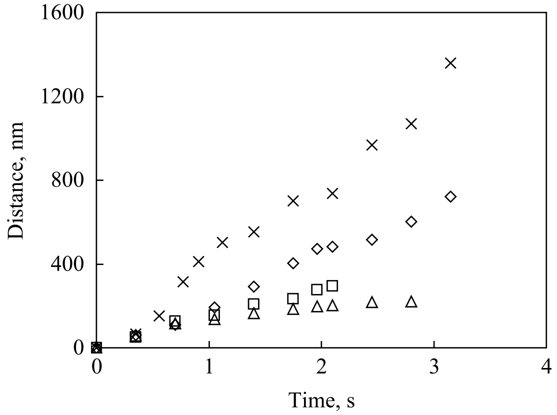

Fig. 3. A graph showing the variation in length with time of the lamellae labelled in Fig. 2. +, Lengthening growth of lamella 'A' growth rate 410 nm s^{-1}; ◇, widening growth of lamella 'A' growth rate 231 nm s^{-1}; □, widening growth of lamella 'B' growth rate 135 nm s^{-1}; Δ, widening growth of lamella 'C' growth rate 76 nm s^{-1}.

The polymer films used in this study are ~1 μm thick, sufficient thickness that a spherulitic morphology is observed. Here we present data showing the growth process observed at the spherulite growth front, the subsequent crystallization through spiral screw dislocation growth of large volumes of material left behind on the surface, and finally the slow growth of a thin layer of uncrystallized material, presumed to be similar to that described in [31]. The primary growth data was obtained on the lower molecular weight polymer (PEO50), as we have been unable to obtain images of sufficient quality to measure growth rates of individual lamellae in the PEO220 during primary growth. The reason for this is unclear, although it is likely that the images obtained of the primary lamellae involve some penetration of the AFM tip into the molten polymer (by several tens of nanometres) and this penetration may not occur in the higher molecular weight polymer, leading to the images of slightly submerged lamellae being indistinct. It should also be noted that this penetration of the tip might lead to some motion of material across the sample surface caused by the process of imaging. We see no evidence of this in any of the data presented (e.g. no preferential growth along the fast scan axis, or any other scanning, rather than sample, related direction), but some influence of the tip on the process being followed is unavoidable when the contrast mechanism derives from the interaction force between the tip and the sample. All of these growth processes are observed at a temperature of approximately 56 °C for the PEO50 sample and 57 °C for the PEO220 sample, where the growth rate of the primary

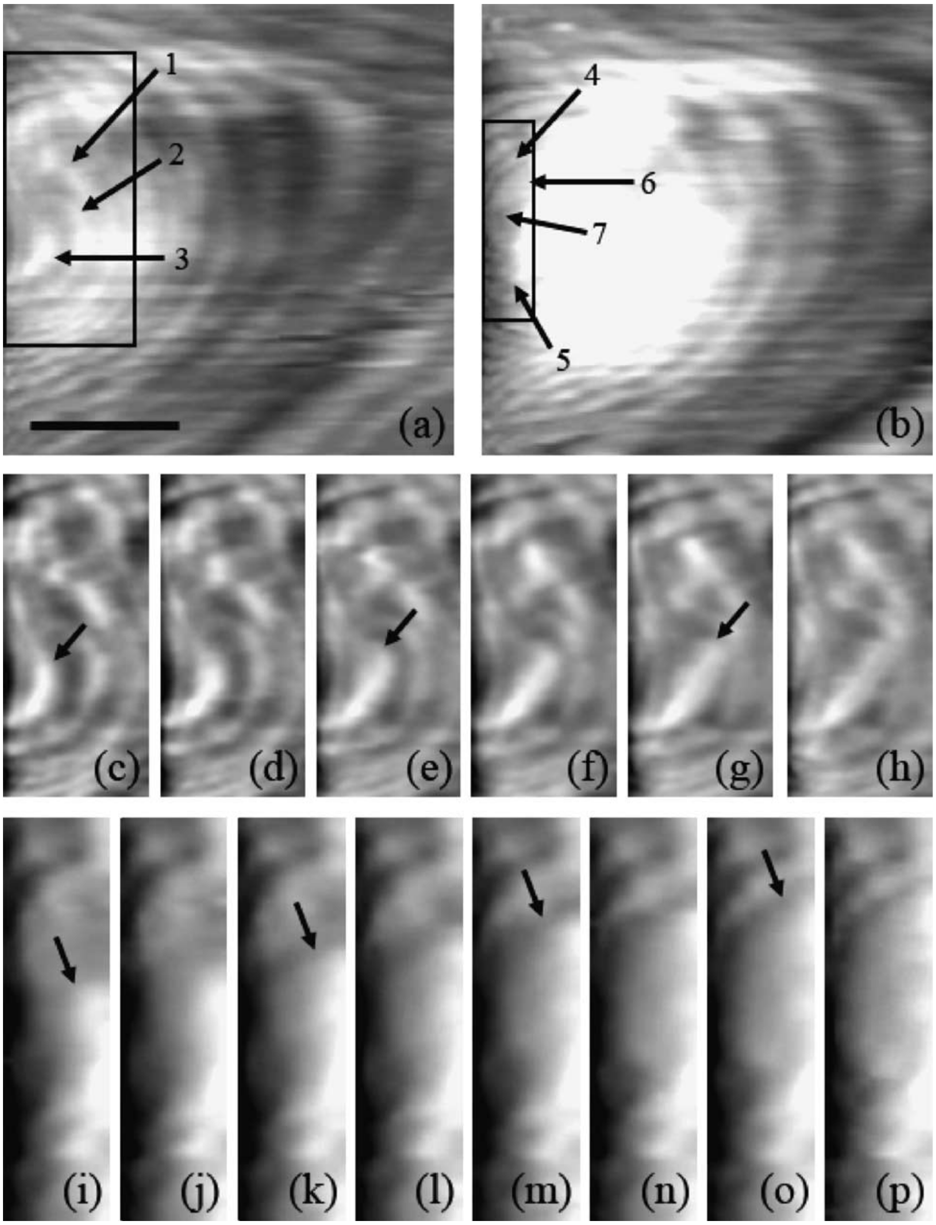

Fig. 4. A sequence of VideoAFM images showing a PEO220 screw-dislocation growing from the melt at a temperature of 57 °C. (a) and (b) show the initial screw dislocation (0 s) and the final screw dislocation after imaging the growth process (3.08 s). The numbers indicate growth terraces referred to in the text. The scale bar represents 500 nm. (c)–(h) are a series of images in which the growth of terraces '1', '2' and '3' can be seen, images collected consecutively at 70 ms intervals. The arrows indicate the advancing growth front of terrace 3 to guide the eye. Each image is 500 nm wide. (i)–(p) are a series of images in which the growth of terrace '6' can be seen. The arrows indicate the advancing growth front to guide the eye. Images collected consecutively at 70 ms intervals. Each image is 250 nm wide. Images (c)–(p) have been processed to enhance contrast as described in Appendix A.

spherulite is $\sim 400\ \mathrm{nm\ s^{-1}}$. This is a growth rate approximately 100 times higher than that studied in most in situ AFM experiments, and, although far from the peak growth rate of PEO, it might be expected that the growth kinetics would be markedly different from those observed previously.

Fig. 2 shows a series of images of the spherulite growth front. The growth tip of the lead lamella is labelled A in the figure. Fig. 3 shows the variation in length with time of this lamella and the variation in width with time (i.e. tangential to the spherulite front) of this and two other lamellae (labelled B and C)—the length and width are indicated by arrows in Fig. 2(b), labelled *l* and *w*, respectively. There is approximately a factor of two between the widening and lengthening growth rates of the lamellae ($231\ \mathrm{nm\ s^{-1}}$ compared to $420\ \mathrm{nm\ s^{-1}}$). In spherulites it is known that lamellae ultimately have an aspect ratio that is considerably greater than the 2:1 that this difference in growth rate would imply. From this we can conclude that the high aspect ratio in the case of PEO spherulites is the result of geometric constraints on the lateral growth of lamellae—as lamellae grow wider, they meet neighbouring lamellae and impinge, preventing further growth in this direction. This provides evidence supporting the view that it is dense branching that leads to the spherulitic texture [32], rather than the fibrillar habit of polymer crystals. There is some variation in the rate of widening between the three crystals. Currently, we have insufficient statistics to determine if this is just a random fluctuation in growth rates, or if it is due to different constraints placed on growth for the different lamellae, coming from the presence of the surface.

Fig. 4 is a series of images taken during the very rapid growth of a screw dislocation on the sample surface. Note that this is taken from a different sample (with a higher molecular weight) than the data of spherulite growth. Screw dislocation spirals are a frequently found surface growth morphology in PEO, occurring for the classical reason that the screw dislocation source allows growth in a slow growing crystal axis (in this case along the chain axis, perpendicular to the lamellar surfaces). The series of images in Fig. 4, part of a series of 47 images collected in 3.3 s, show the evolution of a multi-dislocation growth site (a movie corresponding to this series of images is available at www.infinitesima.com/publications/polymer_aug05.html). Several terraces can be seen to grow simultaneously (numbered in the figure in order of ascending height from the sample surface). As the terraces grow vertically out of the sample plane, the response of the cantilever to the surface needs to become more rapid and some information is lost. To help clarity in the images where contrast is lost, images 5c to 5p are enlargements of the growing terraces. These images have been processed to enhance printed reproduction, the method used and the original, raw data being available in Appendix 1. The image contrast is sufficiently good, however, to allow the change in size with time to be measured for seven individual terraces of the growth spiral (labelled in Fig. 4), as shown in Fig. 5. Table 1 gives the growth rates of these terraces taken from the slope.

The spiral terrace is growing far behind the growth front, so we must assume that there is molten material left behind at the surface that has not previously crystallized because no crystal branch has nucleated to allow growth in the necessary direction. The formation of a screw dislocation allows this material to crystallize, and apparently leads to a large amount of the surrounding melt being incorporated in one vertical growth spiral.

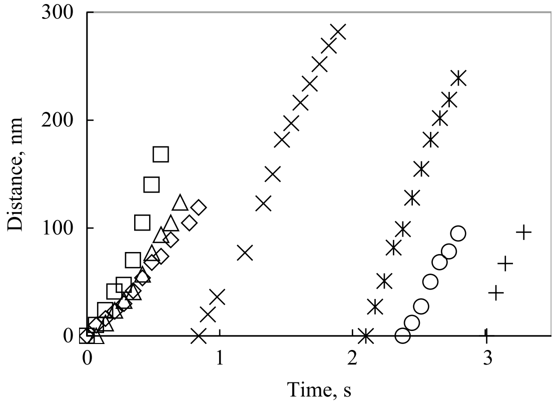

Fig. 5. A graph showing the variation in length with time of the terraces labelled in Fig. 4. ◇, Terrace 1; □, terrace 2; Δ, terrace 3; ×, terrace 4; *, terrace 5; ○, terrace 6; +, terrace 7. The growth rates are given in Table 1.

Table 1
Growth rates measured for each spiral terrace shown in Fig. 4

Terrace number	Growth rate (nm s^{-1})
1	143
2	298
3	196
4	279
5	347
6	234
7	331

The individual numbered terraces are labelled in Fig. 4.

The growth data shows a spread of growth rates for the different terraces from 130 to 342 nm s^{-1}. The spiral growth is occurring vertically out of the sample surface, the growth front of the individual lamellae that make up the spiral presumably being supplied with molten polymer by diffusion over the sample surface, as there is no reason to expect the melt surface to contain sharp bumps of this sort. A priori, we might expect the growth rate to slow as the terraces grow up away from the sample surface, with the lower terraces (e.g. terrace 1 in Fig. 4) growing faster than the upper terraces (e.g. terrace 7) because of the increased rate of diffusion necessary to bring the material up to the top spiral and the lamellar growth front. Instead, there is no trend in growth rate with the number of the terrace, so the transport of material vertically out of the plane of the sample, to feed the growing crystal, is not hindering the growth process noticeably. These growth rates are close to those measured for the primary crystallization (approximately 400 nm s^{-1}), the slightly lower values presumably reflecting the increased diffusive barrier to growth as material must migrate over the sample surface to the growing spiral. However, the fact that upper terraces of the spiral grow at all, rather than the lower terrace growing rapidly to consume all the available material, implies that the process of chain attachment at the growth front is considerably slower than the rate of material transport (otherwise, it would be improbable that a crystallizable chain would pass over available growth sites low down on the spiral to reach the spiral apex). So in this surface crystallization situation, chain attachment rather than diffusion is the main controlling factor. The final morphology is a classic spiral similar to that shown in Fig. 1, helping to confirm that imaging has not interfered with the crystal growth.

Fig. 6 is a series of VideoAFM images of the growth of a crystal structure that occurs after the main growth front has past. The images shown are part of a series of 182 images

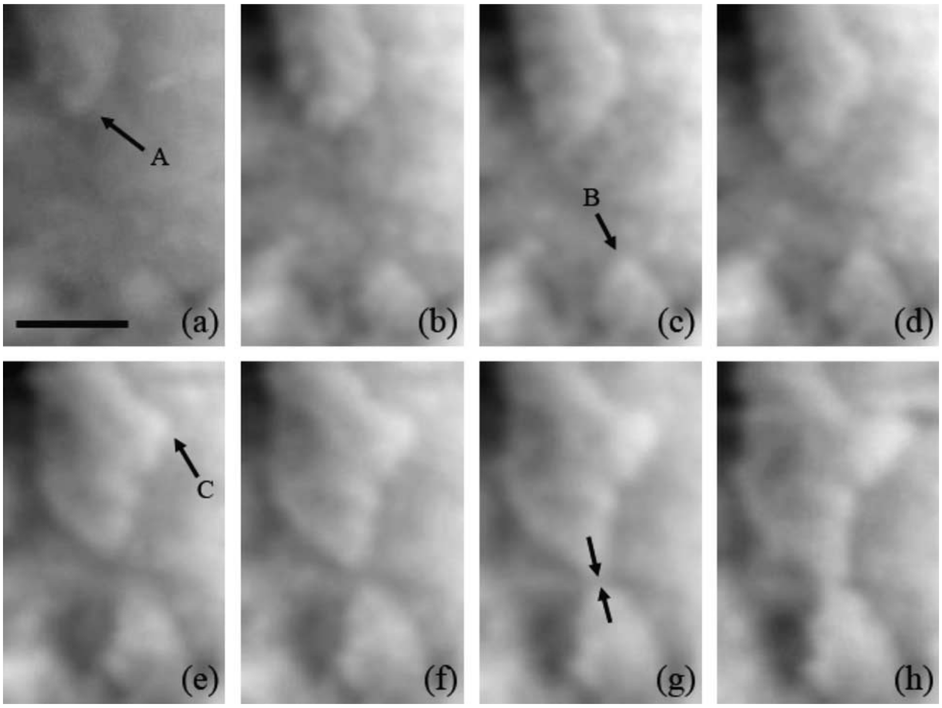

Fig. 6. A sequence of VideoAFM images crystal growth in a thin surface layer of molten material at a temperature of 56 °C. 'A', 'B' and 'C' indicate structures referred to in the text. (a) Taken at 0 s, (b) taken at 0.84 s, (c) taken at 1.54 s, (d) taken at 2.24 s, (e) taken at 3.29 s, (f) taken at 3.71 s, (g) taken at 4.69 s, (h) taken at 6.09 s. The arrows in (g) show the separation when growth starts to slow down. The images have been processed to enhance contrast as described in Appendix A. The scale bar represents 500 nm.

collected in 13 s (a movie corresponding to this series of images is available at www.infinitesima.com/publications/polymer_aug05.html). Two main structures can be seen growing towards each other, labelled A and B, one down from the top of the image and one up from the bottom. To enhance image contrast, the data has been processed as detailed in Appendix A, where the original raw data are also provided. The upper structure branches (labelled C) and the growth of this branch is also seen. This growth form is probably related to the constrained surface growth morphologies observed with optical microscopy in [31], although in that work the film thickness was controlled to be a non-integer fraction of the crystal thickness, while here the film is thicker and the material left to crystallize remains because of the geometric constraint of the surface. Surface decoration of films is commonly observed, although it is often assumed to occur during cooling. Here we show that this highly non-equilibrium growth process occurs as a second stage of crystal growth at the original crystallization temperature (note this data was collected where the primary growth rate is ~ 500 nm s^{-1}).

Several features are of particular interest. Firstly, the morphology itself is a dendritic or seaweed structure (see, e.g. [33]), as can be seen from the curved growth tip, the existence of a characteristic width of the individual growing 'arms' and the side budding of further growth arms. This morphology implies that material diffusion is strongly influencing the rate of growth and the structure, a conclusion that is reinforced by the relatively slow growth rates compared to those in the bulk of the film at this temperature. This surface secondary growth is different from the in-filling growth that is commonly discussed in polymer crystallization, as it is not the crystallization of the material between lamellae, but rather the crystallization of material left at the surface because of the geometrical constraint that the surface introduces. The observation of dendritic growth structures in very thin films (typically less than the lamellar thickness) is commonplace in PEO [21]—indeed this material has been used as a model for general dendritic growth [33]. However, this is the first time that a related structure has been seen in the crystallization of 'thick' films at the sample surface. Note that the growth arms are only ~ 500 nm wide, so would be hard to resolve with optical microscopy, while AFM studies of PEO crystallization are typically performed at a much smaller supercooling, where the driving force for crystallization is less and hence the probability of leaving material behind at the surface is reduced. Even when such material is left, the slow growth rates would most probably allow crystallization in a more classical lamellar texture, rather than this fingering, dendritic morphology. This, then, is a clear example of how rapid growth can lead to unexpected growth morphologies.

It is expected that the presence of an interface will affect the crystallization process. What is surprising is the contrast in the crystallization mechanisms when operating at high supercoolings and at moderately high molecular weight (when compared to the data in [31]). It is also worth noting that it is this secondary, surface crystallization, which will control the ultimate properties of the surface, and hence will strongly influence the properties of a thin film made from PEO.

Fig. 7 shows the variation in size with time for the three arms labelled in Fig. 6. A striking feature of the data is the change in growth rate as the two opposing dendrite arms, A and B, approach each other. There is a significant slowing in growth that starts when the two arms are ∼30 nm apart, as marked in Fig. 6(g). This 30 nm separation is close to the radius of gyration of the polymer used (also ∼30 nm, although this is the 3D Rg, as the film thickness is unknown). It appears that the observed change in growth rate is due to competition between the two growing crystals, at the molecular scale, for crystallizable material. The dendritic morphology is caused by competition for material along the growth front that leads to the initial surface instability and hence fingering growth. The exceptional feature here is that the inherent length scale of the polymeric melt—the molecular size—appears to be directly influencing the growth process during the process of crystal impingement. It appears that the large size of the polymer molecules only starts to directly influence the growth process (beyond the 'continuum' effects on diffusion rates etc.) once individual polymer molecules might be expected to be spanning the gap between the two growth fronts.

We have presented growth data for three dendrite arms, one of which (C) is an offshoot from another, as well as the variation in width with time of one of the arms (A). The growth rates clearly vary between the three arms, with the offshoot being slower as expected for dendritic crystallization—it is competing for material with the main growth tip. The rate of increase in width of arm A is considerably slower than the rates of growth of the tips, as necessitated by the elongated shape of the crystal. In all cases, there are small fluctuations in growth rate with time. The reason for these fluctuations is unclear, but could be either variations in film thickness, variations in temperature (this is unlikely as the rate variations of each arm do not occur at the same time, but the rates of growth are still sufficiently slow that they can all be assumed to be at the same temperature over the timescale of the measurement), or possibly effects due to the interaction with the other growing crystal tips. The other factor that has to be considered in this unusual growth morphology is the role played by the already crystallized material beneath the surface layer. We have no information about the shape or orientation of the crystallites beneath the surface, but most probably the lamellae are oriented parallel to the film surface, as other orientations would lead to visible edges in our images. Considering the molecular weight, this sub-surface crystal most probably contains parts of some of the chains (cilia) that are slowly crystallizing in the images presented, and variations in the distribution of such cilia will have an impact on the growing surface dendrites. The impact of cilia on polymer crystal growth has been considered extensively in the literature (e.g. Ref. [34]). In the current study, such partially crystallized chains must be included in the growing dendrites, and should introduce perturbations in the growth behaviour relative to 'free' dendrite growth. Unfortunately, we do not possess a sufficiently large data set to perform an analysis to test for any such perturbations.

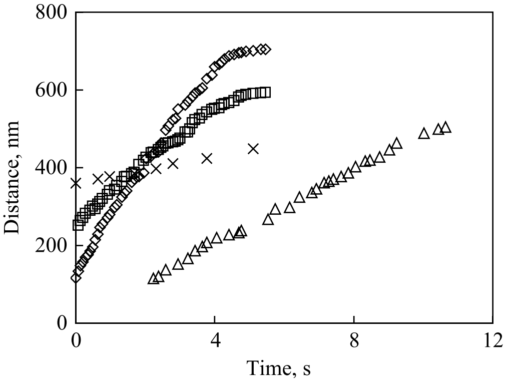

Fig. 7. A graph showing the variation in length with time of the structures shown in figure 6. ◇, The lengthening of the structure labelled 'A'; □, the lengthening of the structure labelled 'B'; Δ, the lengthening of the structure labelled 'C'; ×, the widening of the structure labelled 'A'.

4. Conclusions

This work is the first study of a process using the VideoAFM technique. The VideoAFM allows unprecedented time resolution while maintaining the very high spatial resolution necessary for the study of materials at the molecular scale. It is the only technique available capable of sub-second time resolution and nanometre spatial resolution on soft materials that can image sufficiently large areas to capture rare events.

Measurements of the rates of growth at the lamellar scale within a spherulite front have been carried out under conditions of rapid growth. The ratio of the rate of lengthening to the rate of widening of an individual lamella was found to be approximately two, implying that the highly elongated crystal habit typically found in spherulites are the result of the dense branching morphology and are not a cause of spherulitic growth.

Direct observation of screw-dislocation growth at these high supercoolings confirms that the rate determining step in crystallization is growth front rather than diffusion controlled under conditions of large supply of material. This is the first observation of lamellar scale growth at these rates with sub-optical resolution, and confirms largely similar behaviour to that seen at slower rates with conventional AFM.

The presence of a late crystallizing surface layer of material that crystallizes through a dendritic, diffusion controlled, mechanism was observed. The observation of

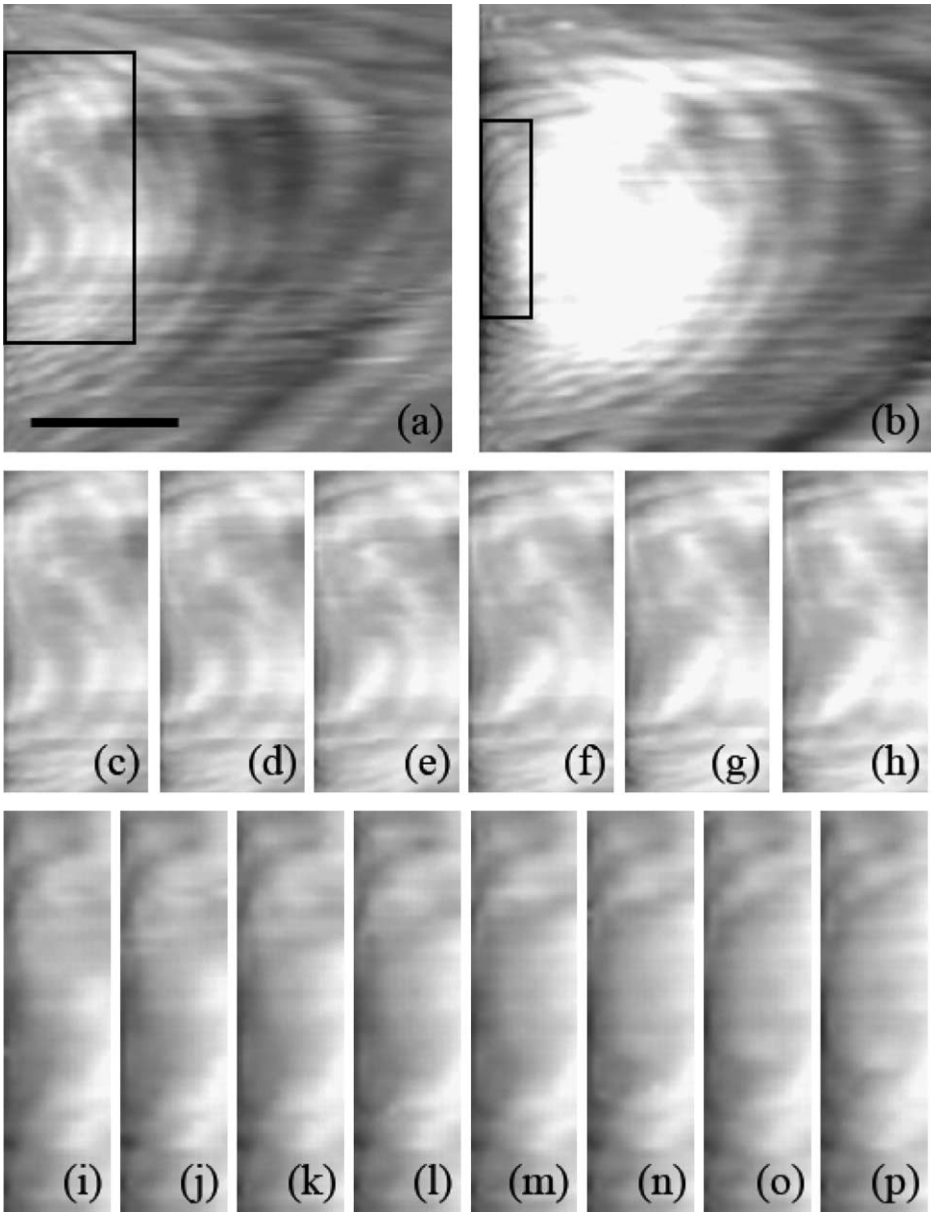

Fig. A1. A series of raw data images corresponding to the data presented in Fig. 4 in the main body of the text.

crystallization at the molecular scale, and the direct confirmation of the competition between growing crystals for material at the molecular level, while at a supercooling comparable to those that might be used commercially, is particularly striking. The possibility of direct observation of spherulitic crystallization, over a wide range of supercoolings where growth rates are comparable to those used in commercial processing, will be an exciting area for future exploration.

Acknowledgements

JKH and CV thank the Engineering and Physical Sciences Research Council, UK, for funding. The authors thank Mr David Catto, Infinitesima Ltd, for instrument support.

Appendix A

Recent availability of image manipulation software makes it more difficulty to draw a line between the enhancement of an image and its distortion [35,36]. The VideoAFM technique used in this article collects data at a rapid rate, working close to the noise. Also, the rate of data capture, and the speed of changing events sometimes mean that a contrast setting that is suitable at the beginning of an image sequence is not optimal by the end. In some cases the raw image data does not contain sufficient contrast that its

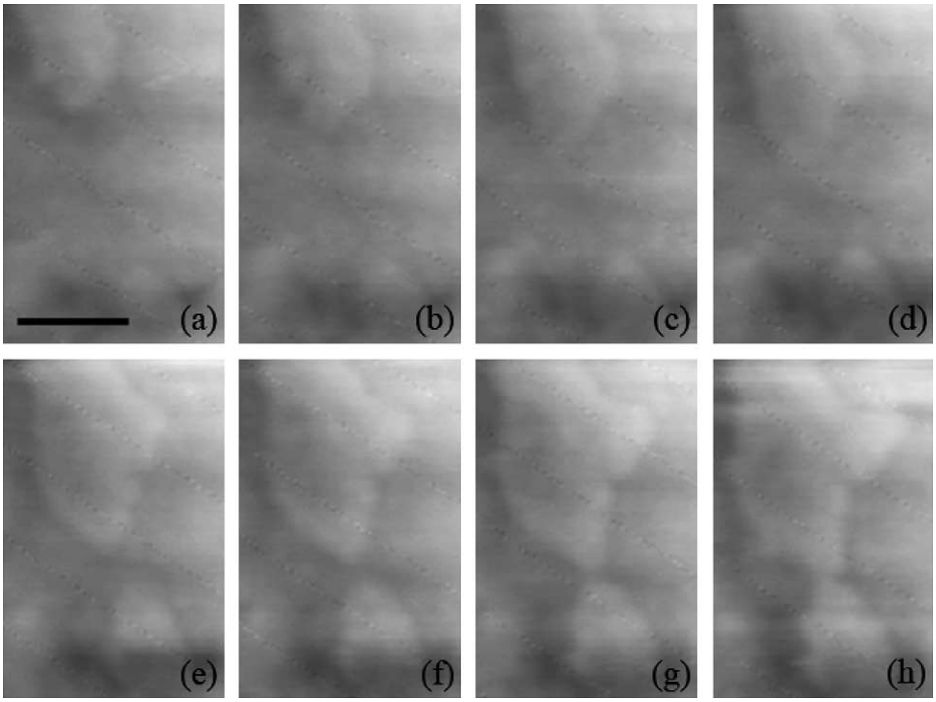

Fig. A2. A series of raw data images corresponding to the data presented in Fig. 6 in the main body of the text.

quality can be guaranteed when reproduced or printed. To enable the images used to be easily viewed, we have used several image manipulation procedures to enhance them that will be detailed in this appendix, the original, un-manipulated images also being included in line with a recent suggestion [35]. However, it should be noted that all the data was analysed and rates etc. measured before image manipulation was performed—the manipulation was carried out only to allow for better reproduction in the printed medium.

As stated in the text, Fig. 2 was filtered to remove horizontal streaks and rescaled, but not otherwise manipulate. Figs. 1(a) and 4(a) and (b) are raw, unprocessed data. Figs. 4(c)–(p) and 6 were processed in ImageJ freeware (a PC version of NIH image, http://rsb.info.nih.gov/ij/) using the following procedure:

(i) Images were first FFT band pass filtered to remove high and low frequency noise and horizontal streaking.
(ii) The resulting image was then processed with the ‘Find Edges’ routine that removes everything except for edges (rapid changes in contrast) from the image.
(iii) The resulting ‘edge’ image was smoothed and then added back into the initial filtered image (i.e. that obtained after process (i)), giving a relatively low noise image with enhanced edges.

Note that when viewing the data as a movie, or when switching rapidly between consecutive images, the brain naturally sees primarily the difference between the images, i.e. the moving edges. Unfortunately, these differences are not so clear when observing an array of static images.

The two figures Figs. A1 and A2 show the raw, unprocessed data corresponding to the processed data presented in Figs. 4 and 6, respectively, in the main body of the text.

References

[1] Welch P, Muthukumar M. Phys Rev Lett 2001;87(21):218302.
[2] Doye JPK, Frenkel D. J Chem Phys 1998;109(22):10033.
[3] Sommer JU, Reiter G. J Chem Phys 2000;112(9):4384.
[4] Keller A. Philos Mag 1957;2:1171.
[5] Terrill NJ, Fairclough PA, Towns-Andrews E, Komanschek BU, Young RJ, Ryan AJ. Polymer 1998;39(11):238.
[6] Strobl G. Eur Phys JE 2000;3:165.
[7] Wang ZG, Hsiao BS, Sirota EB, Srinivas S. Polymer 2000;41(25):8825.
[8] Tracz A, Jeszka JK, Kucinska I, Chapel JP, Boiteux G, Kryszewski M. J Appl Polym Sci 2002;86(6):1329.
[9] Durell M, Macdonald JE, Trolley D, Wehrum A, Jukes PC, Jones RAL, et al. Europhys Lett 2002;58(6):844.
[10] Keith HD, Padden FJ, Lotz B, Wittmann JC. Macromolecules 1989;22:2230.
[11] Hobbs JK, McMaster TJ, Miles MJ, Barham PJ. Polymer 1998;39(12):2437.
[12] Pearce R, Vancso GJ. Polymer 1998;39:1237.
[13] Ivanov DA, Pop T, Yoon DY, Jonas AM. Macromolecules 2002;35(26):9813.
[14] Li L, Chan C-M, Li J-X, Ng K-M, Yeung K-L, Weng L-T. Macromolecules 1999;32(24):8240.
[15] Hobbs JK, Humphris ADL, Miles MJ. Macromolecules 2001;34:5508.
[16] Reiter G, Sommer J-U. Phys Rev Lett 1998;80(17):3771.

[17] Magonov SN, Yerina NA, Ungar G, Reneker DH, Ivanov DA. Macromolecules 2003;36(15):5637.
[18] Pearce R, Vancso GJ. J Polym Sci B 1998;36:2643.
[19] Schultz JM, Miles MJ. J Polym Sci B 1998;36:2311.
[20] Schonherr H, Frank CW. Macromolecules 2003;36(4):1199.
[21] Reiter G. J Polym Sci Polym Phys 2003;41(16):1869.
[22] Sulchek T, Hsieh R, Adams JD, Yaralioglu GG, Minne SC, Quate CF, et al. Appl Phys Lett 2000;76(11):1473.
[23] Barrett RC, Quate CF. J Vac Sci Technol, B 1991;9(2):302.
[24] Walters DA, Cleveland JP, Thomson NH, Hansma PK, Wendman MA, Gurley G, et al. Rev Sci Instrum 1996;67:3583.
[25] Ando T, Kodera N, Takai E, Maruyama D, Saito K, Toda A. Proc Natl Acad Sci 2001;98:12468.
[26] Sulchek T, Hsieh R, Adams JD, Minne SC, Quate CF, Adderton DM. Rev Sci Instrum 2000;71:2097.
[27] Humphris ADL, Hobbs JK, Miles MJ. Appl Phys Lett 2003;83:6.
[28] Humphris ADL, Miles MJ, Hobbs JK. Appl Phys Lett 2005;86: 034106.
[29] Beekmans LGM, vand der Meer DW, Vancso GJ. Polymer 2002; 43(6):1887.
[30] Vancso GJ, Beekmans LGM, Pearce R, Trifonova D, Varga J. J Macromol Sci, Phys 2005;B38(5/6):491.
[31] Reiter G, Vidal L. Eur Phys JE 2003;12:497.
[32] Granasy L, Pusztai T, Borzsonyi T, Warren JA, Douglas JF. Nat Mater 2004;3(9):645.
[33] Ferreiro V, Douglas JF, Warren JA, Karim A. Phys Rev, E 2002; 65(4):042802.
[34] Hosier IL, Bassett DC. Polymer 2002;43(2):307.
[35] Pearson H. Nature News. Nature 2005; 434:953.
[36] Rossner M, Yamada KM. J Cell Biol 2004;166(1):11.